Journal of Low Temperature Physics, Vol. 135, Nos. 5/6, June 2004 (©2004)

Optical Imaging of Helium Interfaces

H. Alles and A.Ya. Parshin*

Low Temperature Laboratory, Helsinki University of Technology, P.O.Box 2200, FIN-02015 HUT, Finland
**P.L. Kapitza Institute for Physical Problems, ul. Kosygina 2, 117334 Moscow, Russia*
Email: harry@boojum.hut.fi

This review describes the development work done in the Low Temperature Laboratory (LTL) at the Helsinki University of Technology which has yielded high-resolution interferometric measurements on various helium interfaces at ultra low temperatures. The optical project was started in the end of 1980s and the free surface of superfluid ^{3}He was seen for the first time ever in 1991. Additionally to the liquid/vapor interface of ^{3}He, also the liquid/solid interface of both ^{4}He and ^{3}He has been the object of investigations. In the course of these studies several important experimental results have been obtained like the discoveries of a new surface state and two new growth mechanisms with ^{4}He crystals, or the observation of a multitude of different facets on ^{3}He crystals. The most significant findings from all these measurements are presented together with the corresponding background information and the details of the experimental setup. At the end of the review we also indicate the plans for new measurements with a faster CCD camera we hope to realize in the near future.

PACS numbers: 07.60.Ly, 67.57.-z, 67.80.-s, 81.10.Aj.

1. INTRODUCTION

In the Low Temperature Laboratory (LTL) the quantized vortex lines were discovered in superfluid ^{3}He immediately after the first rotating nuclear demagnetization cryostat (ROTA I) became operational in 1981.[1] Since then the quantized vorticity of superfluid ^{3}He has been extensively studied in LTL by various methods, the most important of them being the NMR technique.[2] The original impetus for optical studies was the hope of the founder and

0022-2291/04/0600-0665/0

Director of LTL Olli V. Lounasmaa, that the vortex lattice of a rotating superfluid ^{3}He could be seen directly as each vortex produces a dimple on a free surface. The imaging of a free surface of superfluid ^{3}He means, however, optical experiments at submillikelvin temperatures and that is more than an order of magnitude lower that could be reached with conventional optical cryostats where the sample is looked at from room temperature through the windows and thermal filters.[3] Accordingly, the first thing to do was to develop a totally new concept for performing optical experiments at these ultra low temperatures.

The reason why with conventional optical cryostats the temperatures lower than about 20 mK have not been obtained, is simple. The small part of infrared radiation which reaches the sample through several sets of windows and thermal filters, causes of the order of 10 μW heat leak to the sample even in the best optical cryostats. The obvious solution for that problem is to image the sample *inside* the cryostat. For optical imaging of vortex dimples on the free surface of a rotating superfluid just visual observation would not be good enough, and various optical methods were considered in LTL. The use of phase microscopy was studied, for instance, but this method turned out to be too complicated in practice. Thus, a simple two-beam interferometer, where the interference pattern is created by two beams which reflect from the free liquid surface and from the bottom of the experimental cell, was chosen instead.

It should be mentioned here that Professor Frossati's group in Leiden started to prepare for submillikelvin optical experiments in 1987. The Leiden group built a setup[4] for visual studies of ^{3}He crystals. Later this setup was modified in order to make it suitable for studies in high magnetic field.[5] As interferometric techniques have not been applied in Leiden, their resolution has remained low compared with measurements performed in Helsinki.

In this review the progress of the optical project in LTL is followed throughout the years. A special emphasize is on the description of development work on the interferometric techniques which were adapted for imaging the various helium interfaces. The free surface of superfluid ^{3}He was seen for the first time ever in the end of 1991 and soon after that the developed two-beam reflection interferometry was applied also for the studies on the shape ^{4}He crystals. The preparation work for imaging the ^{3}He crystals at submillikelvin temperatures started in 1996 and, as a result, a unique Fabry-Pérot type of multiple-beam interferometer was built inside a nuclear demagnetization cryostat. From all these experiments the most important findings are presented. At the end of the review the present status and the nearest future plans of the optical project are described.

2. OPTICAL EXPERIMENTS ON THE LIQUID/VAPOR INTERFACE OF ^{3}He

2.1. Preparations for Optical Experiments at Submillikelvin Temperatures

The optical project started with a feasibility study and a small dilution refrigerator was built for that purpose. The first task was to investigate the properties of optical materials at low temperatures. The laser light absorption of optical windows made from different materials was measured with a simple but sensitive calorimeter, which consisted of a 0.5 cm^3 piece of copper acting as a heat absorber, and which was connected to the mixing chamber of the dilution refrigerator by a weak link made of a stainless steel tube.[6] Three materials were tested: conventional borosilicate crown glass BK7, sapphire, and fused silica. The thickness of windows was 3 mm and the power of the light beam, transmitted into the vacuum can of the cryostat from a He-Ne laser ($\lambda = 632.8$ nm) at room temperature by an optical fiber, was 20 μW. Absorption by BK7 glass was clearly larger than by the other two materials and on the basis of these results fused silica was chosen as the material of windows of the first sample cell and also of all other optical cells used later.

After these first tests the possibility of using a Charge Coupled Device (CCD) type of sensor of a video camera as a detector of light inside the vacuum can was investigated as well. It was quickly found out that the silicon-based CCDs do not work at very low temperatures, the sensors had to be kept at least $\sim$ 60 K. The thermal radiation from the operating sensor at this temperature could be, however, reduced to a tolerable level of 5 nW and less with suitable thermal filters installed in front of the sensor. For instance, an 8 mm thick calcium fluoride window alone was not a sufficient filter because about 30 nW of thermal radiation was still passing through, and only the addition of a 3 mm thick sapphire window yielded the desired result.[6] It has to be noted that these tests were performed by heating the sensor externally to 60 K as the electrical noise problems did not allow to perform calorimetric measurements when the sensor was switched on. The electrical noise, or actually the heat leak caused by that, was therefore the reason why in the first optical observations on superfluid ^{3}He (see the next section) a fiber bundle was used to transmit the image from inside the cryostat to the video camera at room temperature.

In that small cryostat also the first prototype cell for an optical study on the free surface of liquid ^{3}He was tested. The laser beam illumination was conducted via a beam splitter and lenses through the cylindrical sample cell which had transparent top and bottom windows. The back-reflecting

light was monitored by a Philips LHD 0461/02 video camera with its sensor inside the vacuum can of the cryostat and the connection to the control unit at room temperature was made by a 1.5 m long wiring. The interference pattern could not be seen in these experiments because of surface oscillations; the liquid layer was several mm thick and at the measurement temperature of about 100 mK the viscosity of liquid ^{3}He is too small to damp these oscillations. However, the free surface of liquid ^{3}He could be seen indirectly because the expanded light beam became distorted due to the refraction on the liquid/vapor interface before and after the reflection from the bottom window. The meniscus of a stationary liquid ^{3}He layer was found to be strongly curved due to capillarity forces as the cell diameter was only 7 mm.

2.2. First Optical Observations on Superfluid ^{3}He

2.2.1. Setup for optical experiments at submillikelvin temperatures

Figure 1 shows a schematic view of the optical setup inside a nuclear demagnetization cryostat with which the free surface of superfluid ^{3}He was seen for the first time ever.[7] The main difference with the test setup described in the previous section is that the CCD-sensor is not inside the cryostat, the whole video camera is at room temperature and the light is conducted to the camera by a 2.2 mm diameter coherent fiber bundle (FB) consisting of 30 000 optical fibers.

The source of illumination is a 5 mW He-Ne laser (LA) which rotates together with the whole cryostat. The light emerging from the end of the fiber (F) inside the cryostat is collimated by a convex lens (L3) to a parallel beam of about 2 mm diameter and that beam is guided through the optical cell (OC) by a beam splitter (BS) and two mirrors (M1) and (M2). When passing the cell, the beam diameter is about 10 mm thanks to the two planar-convex fused silica lenses (L1) and (L2). The aim of the adjustments was that the two beams reflected (1) from the free surface of the sample ^{3}He and (2) from the upper surface of the bottom window (WW) of the cell reach the lower end of the fiber bundle. Only a small fraction of the illuminating light is reflected back; more than 90 per cent of light passes the cell and is guided by a mirror (M3) through a hole in the inner radiation shield to the black-painted surface on the outer radiation shield which is thermally anchored to the still (ST) of the dilution refrigerator.

The optical cell is a cylindrical ($\varnothing$ = 20 mm) copper volume sealed by two fused silica windows which are antireflection-coated with magnesium fluoride yielding the reflection coefficient of about 0.01. The top window (TW) is tilted by two degrees and the bottom window (WW) wedged by

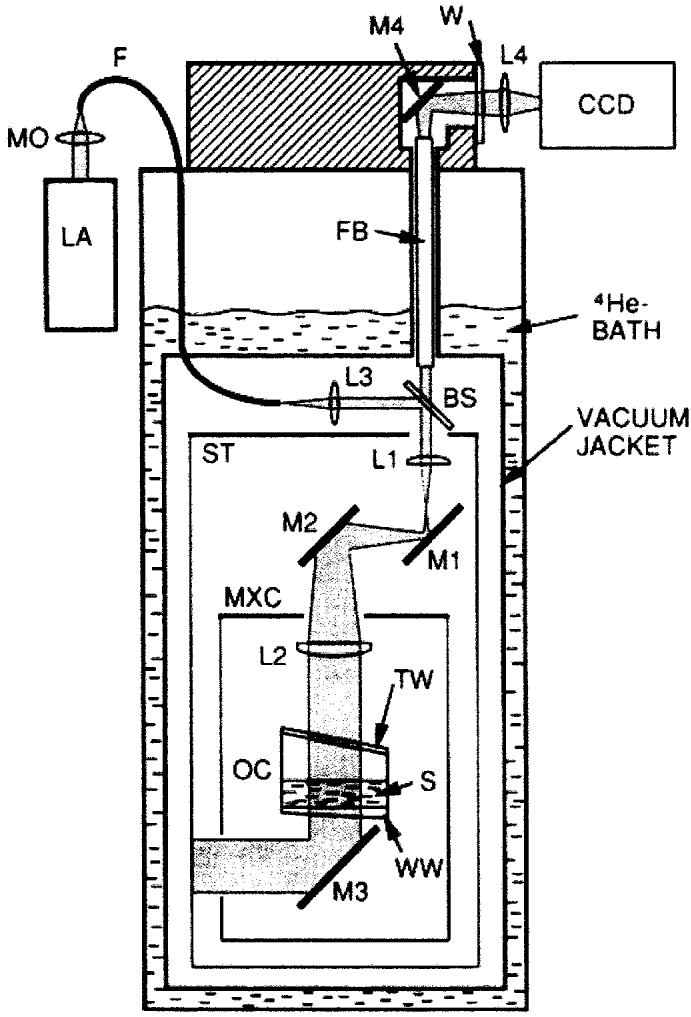

Fig. 1. Schematic illustration of the optical setup inside a nuclear demagnetization cryostat. L1-L4, optical lenses; M1-M4, aluminum coated mirrors; MO, microscope objective; TW, tilted window; WW, wedged window; MXC, mixing chamber. For other abbreviations, see text.[7]

the same degree so that the reflections from the corresponding surfaces do not reach the lower end of the fiber bundle. The thickness of windows is 2 mm and the seals between the windows and the copper body of the cell were made using indium o-rings. The ^{3}He sample (S) is connected to the heat exchanger volume of the nuclear stage (not shown in Fig. 1) through a 1×1 mm^2 hole located just above the bottom window and through a filling tube which has an inner diameter of 4 mm. The thermometry is based on the pulsed NMR measurements on Pt-powder, immersed into the ^{3}He-liquid in a separate tower attached to the nuclear stage. The lowest temperature achieved in these experiments was about 0.7 mK.

For imaging typically 20 ms laser pulses were applied and the images were recorded on the video tape. The interference pattern was only barely visible in printed images due to the very different reflection coefficients (by two orders of magnitude) of the liquid/vapor interface of ^{3}He and of the upper surface of the bottom window. In order to make the fringes clearly visible, two subsequent images were subtracted and in that way Fig. 2 has been obtained.

One has to mention that after the experiment was cooled down, the interference pattern had to be looked for by tilting the whole cryostat in order to get the orientation of the upper surface of the bottom window of the cell close to the plane determined by the free surface of a stationary liquid, i.e., perpendicular to gravity. This was necessary because, in spite of careful adjustments done at room temperature, the different thermal contraction coefficients of materials caused deviations from the original settings. Therefore in these experiments the interference fringes were circular even when the liquid surface was flat, and that was due to the shape of the lower window which was slightly convex. In order to seal the cell, the windows were tightened so much that they were deformed.

2.2.2. Experimental observations

With the setup described in the previous section the huge viscosity change of a ^{3}He-liquid at the superfluid transition ($T_c = 0.93$ mK at zero pressure) was seen directly when the slowly, less than one revolution per minute rotating sample was cooled through the transition. The monitored light beam, which had been reflected from the bottom window of the cell and refracted from the free surface of the liquid, started to precess with the frequency of a rotation immediately after the superfluid transition had been taken place. This was due to the fact that the axis of the cryostat was not perfectly aligned with respect to gravity, and only in a superfluid state the

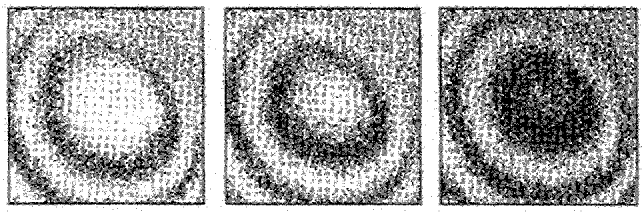

Fig. 2. Fountain effect in a 0.5 mm layer of superfluid ^{3}He. From left to right, the subtracted images (see text) are taken with 20 ms intervals. The shrinking rings indicate an increase in the layer thickness.[7]

free surface of a ^{3}He sample was able to adjust itself perpendicular to gravity thanks to the highly mobile superfluid component. In the normal state the meniscus of a highly viscous normal liquid was determined by the cell walls and no precession of the monitored light beam was seen.

The fountain (or thermomechanical) effect was demonstrated in a neat way in these experiments. A special superleak was not necessary because the normal fluid component of a thin superfluid layer was locked to the bottom of the cell by its large viscosity. Absorption of the illuminating long (a few seconds) laser pulse by the cell windows induced a temperature rise in the liquid which caused a rush of the superfluid component into the illuminated area. In the interferograms it was seen as shrinking of the circular interference fringes towards their center (see Fig. 2). The level rise of a 0.5 mm thick liquid layer, by about 10 μm, took place during illumination while the superfluid sample warmed up into the normal state. In the normal state, the liquid started to relax slowly back, which was seen in the interferograms as expanding fringes.

In rotation, it was found that the surface profile of a rotating superfluid ^{3}He had the same parabolic shape as the rotating normal liquid, $z(r) = \Omega^2 r^2/2g$, where r is the distance from the rotation axis, Ω the angular velocity and g the gravitational acceleration constant.[7] This meant that the rotating superfluid ^{3}He had an equilibrium density of vortices.

The described observations on the free surface of superfluid ^{3}He were the first optical experiments at submillikelvin temperatures meaning a technological breakthrough. The most important physical result obtained was the finding that the meniscus of a rotating superfluid ^{3}He has the same parabolic shape as of the rotating normal liquid. One should note that these were the similar measurements on the meniscus of a rotating superfluid ^{4}He (at much higher temperatures, of course) by Osborne[8] in 1950, in which the first evidence of superfluid vortices was obtained.

2.3. Further Studies on the Dynamics of a Thin Superfluid ^{3}He-Layer

2.3.1. Modifications to the experimental setup

After these first optical observations on superfluid ^{3}He several modifications were made to the experimental setup (see Fig. 3). The main improvement was the installation of a CCD-sensor (Matsushita, MN 3745) inside a vacuum can of the cryostat. The experimental resolution increased by an order of magnitude as there are 518×582 pixels in the sensor compared to 30 000 single fibers in a coherent bundle which was used in the first set of experiments.

Initially that real time (25 frames/s) video camera induced a heat leak of the order of 1 μW to the sample due to rf-radiation. This problem was solved by constructing a "Faraday cage" around the inner parts of the cryostat.[10] As a result, the heat leak due to the digital signals entering the cryostat was reduced below 1 nW. It was also found that the remote operation of the CCD-sensor caused a phase shift of the clock signals due to the extended electrical wires between the sensor and its control electronics at room temperature. That phase shift was compensated by adding two advanced CMOS gates, with a total delay of about 10 ns, into the clock signal line of the CCD read-out control.[10]

The optical scheme was modified so that only a single lens was used to focus the (interference) image to the sensor. The initial scheme (see Fig. 1) had a 2-lens telescope system and due to that the extraction of quantitative data was somewhat difficult. The contrast of the interference pattern was improved by employing a reference wedge, the upper surface of which had a reflection coefficient 3×10^{-4}; this value is close to that of the reflection from the free surface of liquid ^{3}He. This fused silica reference wedge was installed inside the cell and it was pressed only slightly against small pieces of indium to avoid mechanical stresses which had caused the convexness of the reference plane in the original setup.

A bellows system, operated using liquid ^{3}He, was built in order to be able to adjust the orientation of the reference plane during measurements. The optical chamber was supported by two bellows from above (only one of them is seen in Fig. 3) and a third corrugated tube made the connection from below to the heat exchanger volume. Thanks to such a scheme the orientation of the reference plane could be varied up to half a degree by changing the pressure of ^{3}He in the two upper bellows and there was no need to tilt the whole cryostat to get the interference pattern visible as in the first set of experiments.

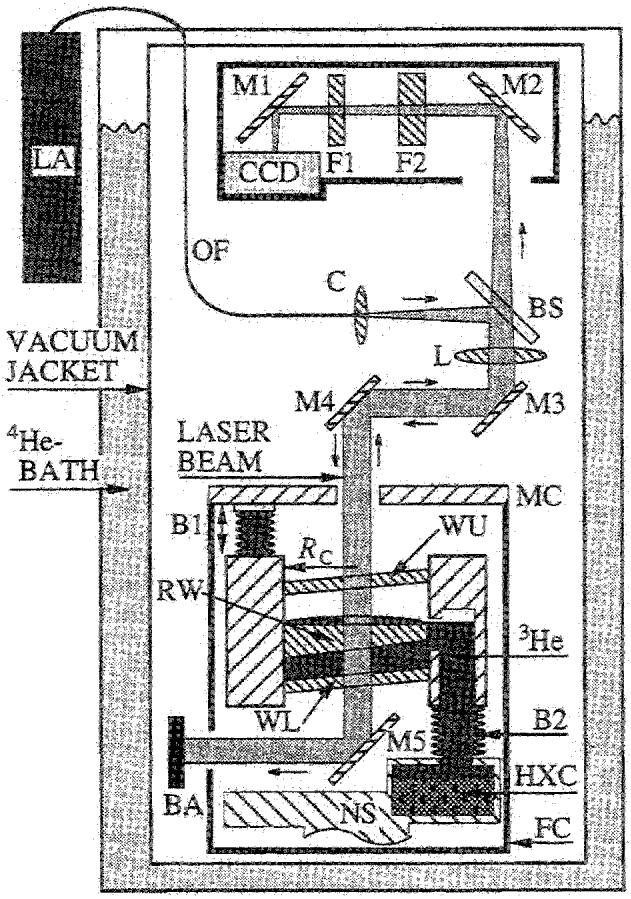

Fig. 3. Scheme of the modified optical setup. L,C, lenses; M1-M5, mirrors; F1-F2, thermal filters; BS, beam splitter; OF, optical fiber; LA, laser; B1-B2, bellows; WU and WL, cell windows; RW, reference wedge; MC, mixing chamber; BA, beam absorber; HXC, heat exchanger; NS, nuclear stage; FC, Faraday cage. The radius R_c of the optical cell is 10 mm.[9]

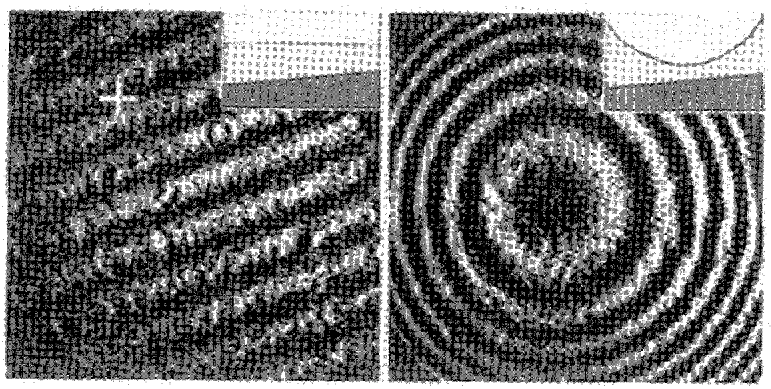

Fig. 4. Interferograms of (a) stationary and (b) rotating ($\Omega = 1.55$ rad/s) superfluid samples of ^{3}He. The adjacent fringes indicate a change in the liquid thickness by $\lambda/2n_l = 310$ nm above the tilted reference glass as illustrated in the insets; n_l is the refractive index of liquid ^{3}He. The white cross in (a) marks the center of the optical cell. The size of interferograms is 5×5 mm^2.[11]

2.3.2. Rotating ^{3}He: Observations on the superfluid meniscus

Figure 4(a) presents an interferogram of a stationary superfluid ^{3}He sample taken with the modified optical setup. Rotation-induced curvature of the free liquid surface becomes evident in the interferograms by moving and bending of fringes. At high speeds, when the curvature of the liquid meniscus is comparable to the tilt of the reference plane (see the insets), circular interference fringes were formed as illustrated in Fig. 4(b).

The surface profile of the liquid could be obtained, in principle, directly from the interferograms. However, it turned out that the most sensitive method, especially at low rotational speeds when the curvature of the liquid meniscus was small, was to follow the liquid depth at the bottom (nadir) of the parabolic meniscus. The spatial shifts of the interference fringes could be resolved within an accuracy of about 1/30 of their width which corresponds to a vertical resolution of 10 nm in the liquid depth.

With that improved resolution, two novel superfluid menisci never seen before were found in ^{3}He.[11] First, at low rotational speeds below about $\Omega = 0.2$ rad/s, the vortex-free Landau state with a reduced temperature-dependent meniscus was observed (see Fig. 5). A deeper-than-expected

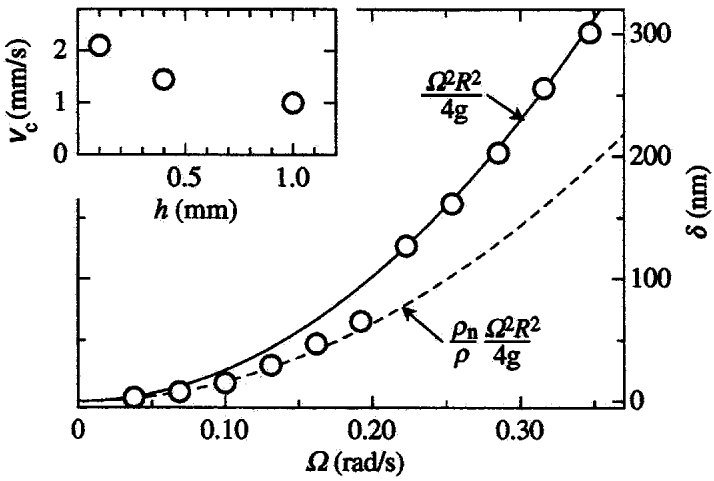

Fig. 5. Liquid depth change $\delta = |z(0)|$ measured during acceleration for a 0.1 mm thick layer of ^{3}He. The solid and dashed curves mark the calculated behavior for an equilibrium rotation and for a vortex-free superfluid at 0.68 T_c, respectively; R is the radius of the cylindrical optical cell and ρ_n/ρ is the relative amount of normal liquid. In the inset the maximum counterflow velocity v_c at the wall of the cell is presented as a function of film thickness h.[11]

meniscus was seen after a rapid halt of the cryostat when the normal liquid stopped during a short relaxation time and the decay of a superfluid circulation was followed. The depth of that exotic meniscus was explained by a reactive radial force between the rotating superfluid and the stationary normal liquid.[11]

Additionally to the measurements with a rotating superfluid, the dynamics of a thin layer of superfluid ^{3}He was studied also in a stationary state. A pair of light pulses was employed: the first pulse was applied to excite the liquid level thermomechanically while the second pulse probed the height of the liquid surface after a short time interval. By varying the time between pulses, the impulse responses of thin superfluid layers at various temperatures could be constructed which yielded the value of the second viscosity in superfluid ^{3}He.[9]

2.4. Attempts to Observe the Vortex Lattice in ^{3}He/^{4}He Mixtures. Nonwetting Phenomena

The resolution of the applied interferometric method achieved in LTL was not enough to observe the individual vortex dimples on the free surface of a rotating superfluid ^{3}He as the depth of these dimples should be of the order of 1 nm.[12] It has been calculated, however, that in a rotating phase-separated liquid ^{3}He/^{4}He mixture the vortices in the ^{4}He-rich superfluid phase should produce dimples of about 60 nm depth as the surface tension of the interface between the ^{3}He-rich and ^{4}He-rich phases is by an order of magnitude lower than that of the free surface of superfluid ^{3}He.[13]

Several attempts were made to observe the vortex lattice on the interface of a phase-separated liquid ^{3}He/^{4}He mixture, but no fingerprints of vortices were found. The reflection from the phase separation interface was too weak to be observed when there was a free liquid surface (with a larger reflection coefficient) in the cell. When the cell was filled completely, i.e., there was no free liquid surface present, the phase-separation interface was vibrating too much for accurate observations even in a stationary state. Attempts to detect vortex dimples were thus unsuccessful.

In the course of these studies with ^{3}He/^{4}He mixtures, however, an interesting nonwetting behavior was found. In the phase-separated mixture films the upper ^{3}He-rich phase did not wet the lower ^{4}He-rich phase under a small continuous feed of ^{4}He atoms to the vapor phase.[14] Instead, under this dynamic situation, floating pools of the ^{3}He-rich phase were stabilized with a contact angle of the order of 10^{-2} rad. In equilibrium, the concentrated ^{3}He-rich phase was observed to be nucleated uniformly on the free surface, i.e., wetting completely the lower ^{4}He-rich phase.

Nonwetting phenomena were later observed also in the experiments with pure superfluid ^{4}He. In contrast to the expectations, superfluid ^{4}He was not able to wet a smooth fused silica window covered by a multi-layer antireflection coating whose topmost layer was from magnesium fluoride.[15] The measured contact angles displayed spatial variation, hysteresis and strong history dependence. This result was later explained by a spatially varying distribution of vortex lines.[16]

3. SUPERFLUID/SOLID INTERFACE OF HELIUM

Helium crystals provide a good model system for verification of different theoretical concepts concerning both the static and dynamic properties of the crystal surface such as an equilibrium crystal shape, surface phase transitions, 2- and 3-dimensional nucleations, elementary mechanisms of the

crystal growth, etc. The main advantage of helium is, first of all, the unique possibility to investigate its liquid/solid interface at arbitrarily low temperatures, when thermal effects become negligible and quantum phenomena start to play a major role. As a result, the relaxation times become very short, which is necessary for accurate studies and crystals can grow very fast even under small departure from equilibrium. Due to this last point, almost perfect large crystals can be easily grown.

3.1. Experimental Studies with ^{4}He Crystals

The studies with ^{4}He crystals started in parallel with the experiments on the free surface of superfluid ^{3}He which were carried out in a big demagnetization cryostat as the small test cryostat was adapted for that purpose. Later these experiments were transferred to the big cryostat and the superfluid/solid interface of ^{4}He was investigated down to 2 mK.[17]

3.1.1. Experimental setup

The optical scheme for studying the shape of ^{4}He crystals was similar to the one used in the experiments on the liquid/vapor interface of ^{3}He, i.e., two-beam reflection interferometry was applied. The main difference was that more sensitive slow-scan STAR-I camera[18] (the same type as used by the Leiden group) was applied instead of the real-time camera. This was necessary because in helium the liquid/solid interface has roughly two orders of magnitude smaller reflection coefficient than the liquid/vapor interface. The image was read from the sensor to the control unit of the camera and transferred to a computer for storage and digital image processing. The example interferogram of the surface of a ^{4}He crystal is shown in Fig. 7.

In addition to the interferometer, a high-precision capacitive pressure gauge and a crystal level gauge were employed. The pressure gauge is of Straty-Adams type,[19] consisting of a 0.3 mm thick Be-Cu membrane ($\varnothing$ = 9 mm) with a resolution up to 12 pF/bar which corresponds to 0.3 μbar resolution in pressure measurements. The commercial Andeen-Hagerling 2500A bridge[20] was used for the measurements of the capacitance of the pressure gauge. The interdigital capacitor, intended for the crystal height measurements, was produced by evaporating a fingered chromium structure on a fused silica substrate. The width and spacing of fringes are 10 μm. The capacitor was mounted to the inner wall of the cell in a bakelite holder, with its fingers vertically. The capacitance of the level gauge was measured using a home-made capacitance bridge, consisting of a signal source, a ratio

transformer and a lock-in-amplifier. The resolution for the crystal height measurements was of the order of 1 μm. The vertical resolution of the interferometer on the crystal shape was about 3 nm in the best cases and this was achieved by an accurate analysis of the intensity variation of fringes.[17]

The crystals were nucleated either spontaneously, or, in order to obtain a crystal seed in the field of view, by the means of a nucleator to which a high voltage was applied. The nucleator is a bifilar coil wound around a bakelite holder, placed just outside the field of view. The crystals were grown and melted by varying the pressure in the cell through the fill line from the ballast volume at room temperature. The temperature was measured in these experiments with a carbon resistor which was calibrated against the melting curve and nuclear orientation thermometers.

3.1.2. Profile of a ^{4}He crystal near the edge of a facet

Measurements of the equilibrium crystal shape give important information about the anisotropy of the surface tension of crystals. This anisotropy is caused by the underlying lattice, and due to that crystals show smooth flat facets on their surface. Of a special interest is a shape of the crystal surface near the edge of a facet. Such a vicinal surface, tilted by a small angle with respect to the facet, may be considered as a stepped surface if elementary steps are well separated. In this case the surface tension and thus also the equilibrium surface profile of a crystal are determined by the step-step interaction at long distances d between steps. The current theory predicts a power law for this interaction ($\sim d^{-2}$);[21] correspondingly, one expects $\zeta \sim x^{3/2}$ for the surface profile near the facet edge.

Figure 6(a) depicts the measured surface profile of a hexagonal close packed (hcp) ^{4}He crystal near the (0001) facet (or c-facet).[22] The facet is shown on the left side at $\zeta = 0$. Far away from the edge the crystal profile follows the gravitational horizon indicated by the dashed line. Figure 6(b) shows a magnified view of the same crystal profile near the facet edge. There are two remarkable features. Firstly, in the slope of the profile is a clear discontinuity (marked by an arrow) which separates two regions with different spatial dependence. In the right-side region, the profile of a crystal surface could be fitted with the form $\zeta \sim x^{\alpha}$, where $\alpha = 1.3...1.8$ and this agrees with the expected behavior of a vicinal surface. Secondly, in the left-side region, which should be attributed to the facet itself and thus should be flat, the profile clearly deviates from a straight line. The measured deviation can be described with the exponent $\zeta \sim \exp(-x/x_0)$, where x is the distance from the facet edge and x_0 is a temperature-dependent constant. This ob-

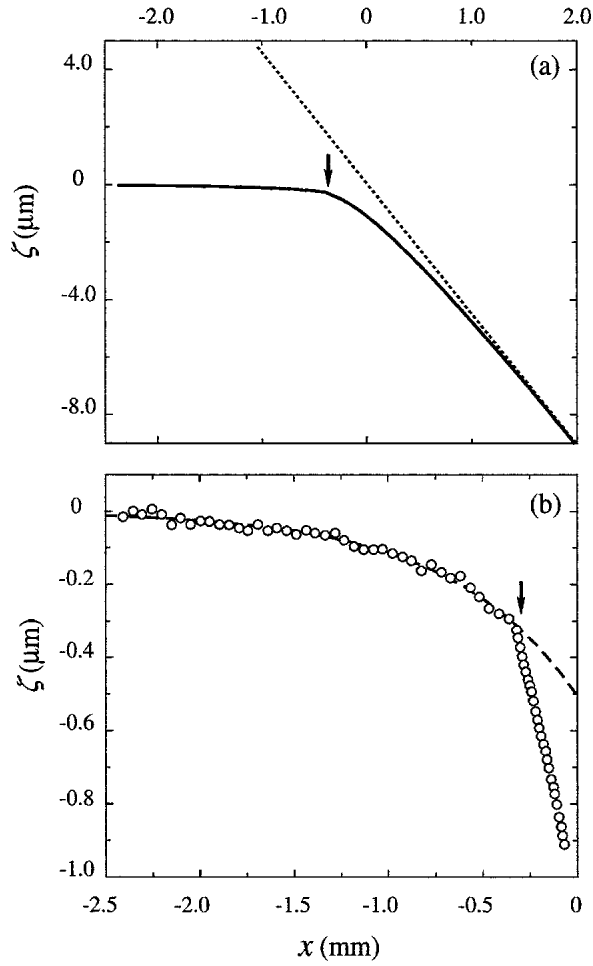

Fig. 6. Surface profile of a ^{4}He crystal at 50 mK (a) in a wide angular region $0 \leq \Theta \leq 4.5$ mrad; the dashed line corresponds to the gravitational horizon and the arrow indicates the slope discontinuity, and (b) at small Θ (magnified view); the line is an exponential fit (see text).[22]

servation demonstrates the existence of a new surface state at the surface orientations very close to the (0001) plane. The slope discontinuity between the "curved facet" and the usual vicinal surface indicates that this new state appears through a first order phase transition.[22]

The new surface state could be attributed to some surface reorganization which could take place through the collective behavior of Frank-Read sources or other surface defects,[23] superfluid flow[24] or logarithmic step-step interactions. However, in order to explain the experimental results, one has to admit a too high density of the surface defects or, respectively, a too high superfluid velocity. Furthermore, the observed slope discontinuity remains unexplained. As for logarithmic step-step interactions, it would be possible in the case of spontaneous transformation of the surface into a new state where the natural rotational symmetry C_3 in the (0001) basal plane is broken (with the bulk symmetry remaining unchanged).[25] With some additional assumptions, concerning in particular the temperature dependence of the parameters of this new state, one could explain the experimental observations by this mechanism. However, there is no other indication of such a surface reconstruction on helium crystals. One more possibility would be the polarization of thermally excited dislocation loops terminating at the boundary,[26] but the activation energies become questionably high in this case. Thus no satisfactory explanation to the origin of the observed new surface state exists at the moment.

3.1.3. Observation of small bundles of dislocations

As mentioned in Section 2.4, the low temperature interferometric techniques developed in LTL did not allow for observations of vortex dimples on a free surface of a rotating superfluid. On the liquid/solid interface similar dimples are formed when a single screw dislocation (or a bundle of them) terminates on the crystal surface. Owing to the strong anisotropy of the surface stiffness,* the depth and shape of such a dimple depend strongly on the surface orientation. In the most favorable case of a vicinal surface on a hcp ^{4}He crystal, tilted by an angle $\sim 10^{-2}$ rad with respect to the c-facet, the depth of such dimple could be up to 60 nm.[27] In measurements with ^{4}He crystals some interferograms display unexpectedly large dimples (see Fig. 7).[28] The reconstructed dimple profile is presented in Fig. 8; its shape is in reasonable agreement with theoretical expectations and the total volume of the dimple, $3 \cdot 10^{-7}$ cm^3, corresponds to a bundle of about 10 dislocations.

*The surface stiffness is the sum of the surface tension and its second derivative with respect to the surface orientation.

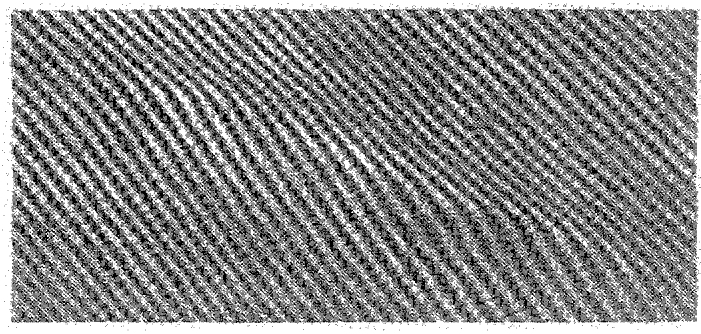

Fig. 7. Interferogram of a surface of a ^{4}He crystal at 500 mK with a large dimple (see the corresponding surface profile in Fig. 8); the inclination of the imaged surface with respect to the c-facet is $5 \cdot 10^{-3}$ rad. The displayed area is 3.0×1.4 mm^2.[28]

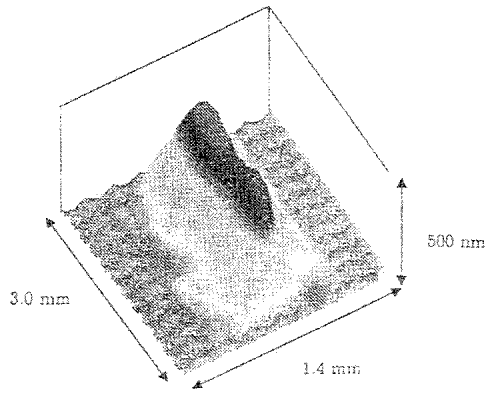

Fig. 8. Dimple profile on the crystal surface (shown as inverted) obtained from the interferogram in Fig. 7.[28]

3.1.4. Nucleation of ^{4}He crystals

The transition from liquid to solid is of first order and a potential barrier caused by the surface tension has to be overcome when nucleating the crystal from metastable (overpressurized) liquid. For usual crystals, it is possible owing to thermal fluctuations. As for helium crystals, where the amplitude of quantum fluctuations is very large, the nucleation via quantum tunnelling becomes possible. In this case, the well-known Arrhenius law, typical for thermal nucleation, should change to a temperature-independent nucleation rate.[29]

According to theoretical estimates, for homogeneous nucleation (thermal or quantum) very high overpressures of the order of 10 bar or even higher are necessary. In practice, however, the nucleation takes place on the walls of the experimental cell and some special wall defects should exist to allow for nucleation at overpressures of the order of a few mbar as observed in experiment (see Ref. 30 for a review).

In LTL the first detailed study of the formation of ^{4}He crystals from the liquid phase was performed.[31] It was found that the nucleation site persisted at a fixed temperature if the pressure of ^{4}He was not decreased more than about 10 mbar below the melting pressure (so-called "memory effect"). Below 100 mK the nucleation rate was observed to be temperature-independent. These observations, together with the analysis of statistical nucleation-event distributions, agree with the theoretical model which suggests that the formation of solid is driven by quantum fluctuations from a seed preexisting in a cavity on the wall.[31]

3.1.5. Spiral growth of ^{4}He crystals

The growth dynamics of facets on helium crystals was studied as well.[17] In classical crystals, facets can grow due to the presence of screw dislocations, terminated on the facet - this is the well-known spiral growth when an elementary step winds around a dislocation line to produce a spiral.[32] Then the growth velocity of the whole facet is proportional to the step mobility and to the square of the driving force. In helium crystals, this growth mechanism also dominates at low temperatures, but shows quite unusual features. It was observed that in the millikelvin region the step velocities can be very high, up to 100 m/s, which is comparable to the sound velocity.[33] Under these conditions, two new features have to be taken into account: the step inertia and the localization of steps at large driving forces.

Figure 9 shows the measured growth velocities of c-facets on ^{4}He crystals at different temperatures. Three different growth regimes are clearly

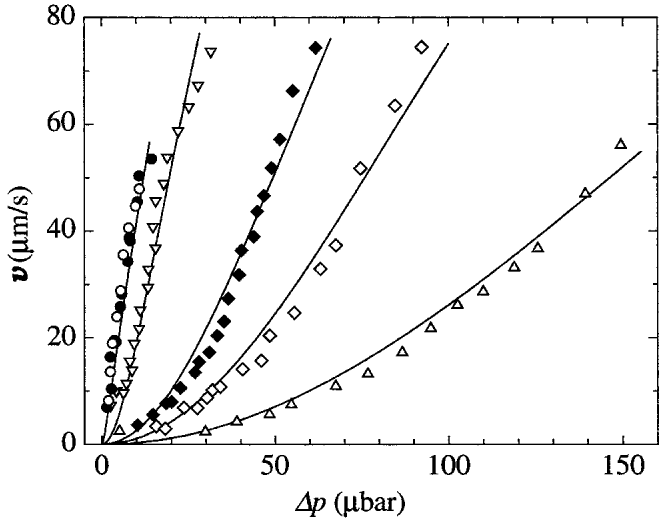

Fig. 9. The velocity v of a c-facet on ^{4}He crystals as a function of the applied overpressure Δp: $T = 2$ mK (o), 20 mK (•), 50 mK (▽), 100 mK (♦), 150 mK (◇), and 200 mK (△). Solid lines are just to guide the eyes.[33]

seen: (1) a classical quadratic dependence of the growth velocity on the applied overpressure at higher temperatures and low velocities, (2) a linear dependence at low temperatures (inertial regime, when the growth speed does not depend on the step mobility), and (3) a tendency to saturate at high velocities due to the effect of localization.[33]

Extremely high mobilities of elementary steps on the facets of ^{4}He crystals provide an opportunity below 100 mK to probe the step structure by impurity atoms of ^{3}He. Indeed, it was found that already very small concentrations of impurities, in the range of 10 to 100 ppm, significantly decrease the step mobility (see Fig. 10).[34] The impurity-step scattering cross-section depends on the effective width of the step, which thus can be derived from the spiral growth data. A value of this effective width was obtained from the data in Fig. 10 and it turned out to be unexpectedly high, about 10 nm (assuming the width to be $\sim 2\xi$, where ξ is the root mean square of the step fluctuations). This was explained as an effect of quantum zero-point oscillations of the step, which significantly enlarge the effective step width.[34]

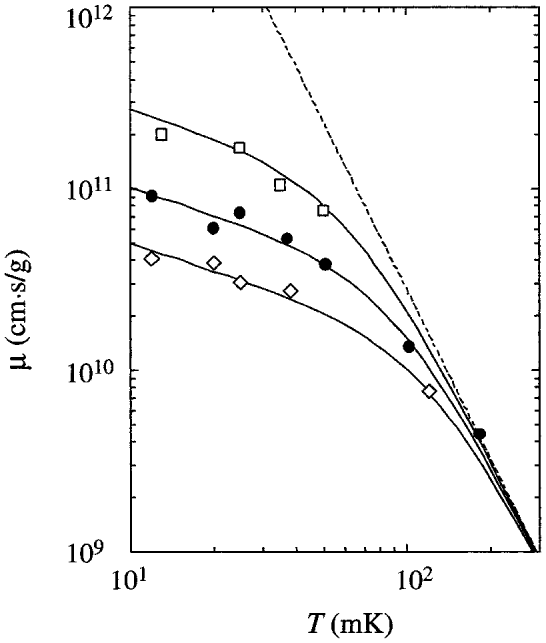

Fig. 10. Step mobilities μ on the c-facets, calculated from the measurements with different ^{3}He concentrations of 40 ppm (□), 110 ppm (•), and 220 ppm (◊). The dashed line represents the data taken with regular ^{4}He (0.1 ppm).[17] The solid lines denote theoretical curves, obtained using an effective step width of 10 nm (see text).[34]

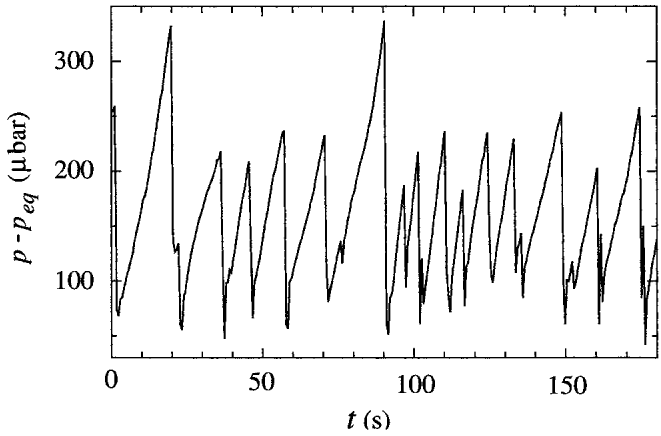

Fig. 11. Pressure trace during growth of a ^{4}He crystal without screw dislocations with the average speed of 170 nm/s. At the instability points the crystal grows abruptly by 200 to 2000 atomic layers.[33]

3.1.6. Two new growth modes found with ^{4}He crystals

Spiral growth of a crystal facet is possible only in the presence of screw dislocations or Frank-Read sources. In this case the applied overpressure should first increase to a threshold level and then stabilize to a value depending on the growth rate. In helium crystals with small number of dislocations this threshold is very low, typically of the order of 1 μbar. Such crystals were obtained in LTL by warming the ^{4}He crystals which were nucleated at 20 mK, above 200 mK.

The growth of the freshly-nucleated crystals, however, produced pressure traces which are shown in Fig. 11 and could not be explained by spiral growth (nor by 2-dimensional nucleation which is known to take place at high temperatures).[33] The pressure of the ^{4}He sample increased almost linearly up to some instability value and dropped then fast by about 100 μbar in less than a second. Such a pressure drop corresponds to a very fast growth of the facet by 200 to 2000 atomic layers. The average threshold for this "burst-like" type of growth was about 200 μbar at 2 mK and it was observed to increase to 1 mbar at 250 mK. With further warming that threshold dramatically decreased to a very low value, and the pressure trace started to show typical spiral growth behavior. Thus it seems reasonable to argue that these crystals did not contain any screw dislocations emerging on the c-facet immediately after the nucleation.

The nature of the burst-like growth mode is still unclear. It is even unknown, whether this growth mode is an intrinsic property of the facet itself or a result of some anchoring of the crystal surface on the wall of the experimental cell. Future experiments should clarify that.

In the experiments on the burst-like growth, during the sections of increasing pressure between the instability points, a slow, continuous movement of the interference fringes was found. The c-facets were able to grow wth small speeds up to 0.5 nm/s, the speed changes being approximately linear with respect to the overpressure. Rising temperature as well as the addition of ^{3}He impurities slowed down the growth speed. The explanation of this growth mode was suggested recently by Andreev and Melnikovsky.[35] They propose that helium crystals can grow "from the bottom", i.e., the facet can move upwards along with the crystalline lattice owing to the motion of vacancies in the crystal. They also predict the existence of a maximum in the temperature dependence of the growth velocity (when there is no zero-point vacancies in helium crystals). It would be very interesting to check this prediction experimentally.

3.2. Optical Studies with ^{3}He Crystals

The reflection interferometry, very successfully applied and developed in LTL at ultra low temperatures, has really high vertical resolution and it has proved to be a great tool to study nearly flat surfaces like the free surface of liquid ^{3}He and the c-facet of ^{4}He crystals.[36] However, with that method, due to the low reflectivity of helium interfaces, only a very small part of the illumination is used and at submillikelvin temperatures the heat load of the applied illumination could be critical. Thus, for optical studies on the crystallization of ^{3}He down to the lowest possible temperatures the path interferometry was considered because it needs much less illumination. The disadvantage of path interferometry compared with reflection interferometry is its much lower resolution, but at the same time the whole shape of the crystals could be observed.[37]

3.2.1. Fabry-Pérot interferometer and the experimental cell

The multiple-beam path interferometry which was chosen for imaging the ^{3}He crystals allows somewhat increased precision compared with two-beam path interferometry due to the sharper fringe shape. However, the most desirable quality of a Fabry-Pérot type of multiple-beam interferometer lies not in the sharper fringe shape, but in the simplicity of its measurement

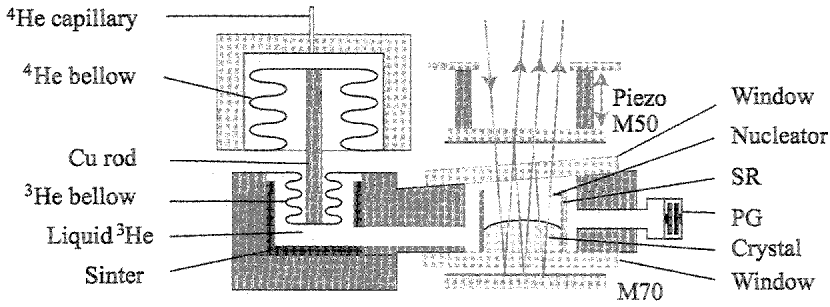

Fig. 12. Schematic view of the experimental cell and a Fabry-Pérot type of interferometer. M50 and M70, mirrors with 50% and 70% reflectivities; PG, pressure gauge.[38]

geometry as it requires only two parallel mirrors. For cryogenic environment, where there is typically little space available, that property is very useful indeed.

Figure 12 shows a scheme of the Fabry-Pérot type of interferometer which was built inside a nuclear demagnetization cryostat in place of the two-beam reflection interferometer. The two semitransparent mirrors of the interferometer are located above and below the optical part of the cell. The top mirror can be moved in vertical direction thanks to the piezoelectrical crystal to which the mirror is glued and that allows to apply phase shift techniques.[37,38] The interference pattern is created between the multiple reflected beams which have travelled through the cell and after that refracted through the upper mirror. The interferograms are recorded by a slow-scan CCD-sensor inside the vacuum can as in the experiments with ^{4}He crystals.

The optical scheme inside the vacuum can was slightly modified: the incoming and outgoing optical arms were made more separated and that simplified optical adjustments. Most of the optical components were housed below the mixing chamber to minimize the optical path length between the end of the fiber and the interferometer. These components are thermally anchored to the cold plate (at about 70 mK) in order to reduce the heat load to the mixing chamber of the dilution refrigerator.

The experimental cell (see Fig. 12) is of the Pomeranchuk type with a total volume of about 13 cm^3, it uses bellows operated with ^{4}He, which allow to vary the cell volume by 8%. This is necessary because, on the melting curve below 320 mK, the pressure of ^{3}He cannot be changed from room temperature as there will be a solid plug in the fill line. The ^{3}He crystals are grown in the cylindrical ($\varnothing$ = 16 mm, h = 12 mm) optical part of the cell. The crystals could be nucleated in the field of view by applying a high

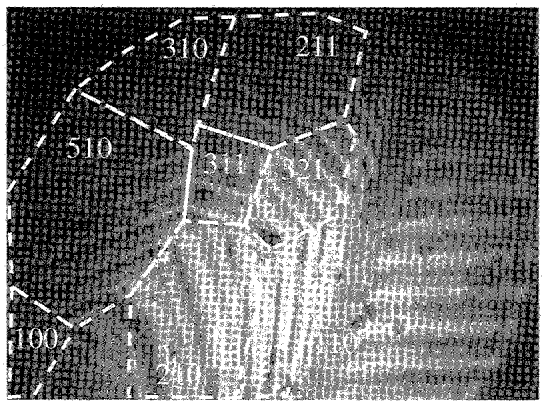

Fig. 13. Interferogram of a growing body-centered cubic (bcc)^{3}He crystal (on left) at 0.55 mK. The facets correspond to the regions with straight parallel equidistant fringes and are labelled with Miller indices. Adjacent fringes indicate a change in the crystal thickness by $\lambda/2(n_s - n_l) = 190$ μm, where $n_s - n_l$ is the difference in the refractive indices of solid and liquid ^{3}He.[43]

electrical field to the sharp tungsten tip which is supported by a Stycast ring (SR) with a diameter of 18 mm. To the cell are connected also the pressure gauge (similar to the one used in the studies with ^{4}He crystals) and the vibrating wire unit. The viscosity measurements with the vibrating wire yield directly the temperature of liquid ^{3}He.[39]

3.2.2. Discovery of many different types of facets on ^{3}He crystals

According to Landau,[40] crystals should show many different types of facets at low temperatures (for a modern theory, see Ref. 41). However, on helium crystals only three different types of facets had been seen both in ^{4}He and ^{3}He before the first set of experiments in LTL with ^{3}He crystals in which many different types of facets were found in 1999.[42] In fact, as the complete analysis of data was not done immediately, it was almost a year later when this discovery was made explicit. Figure 13 displays an interferogram of a growing ^{3}He crystal, where eight facets have been identified, but the total number of different facets observed was eleven.[43]

In these experiments also the growth velocities v of most of the observed facets were measured as functions of overpressure δp.[44] Figure 14 shows the results of a growth sequence with a single ^{3}He crystal; the data points follow

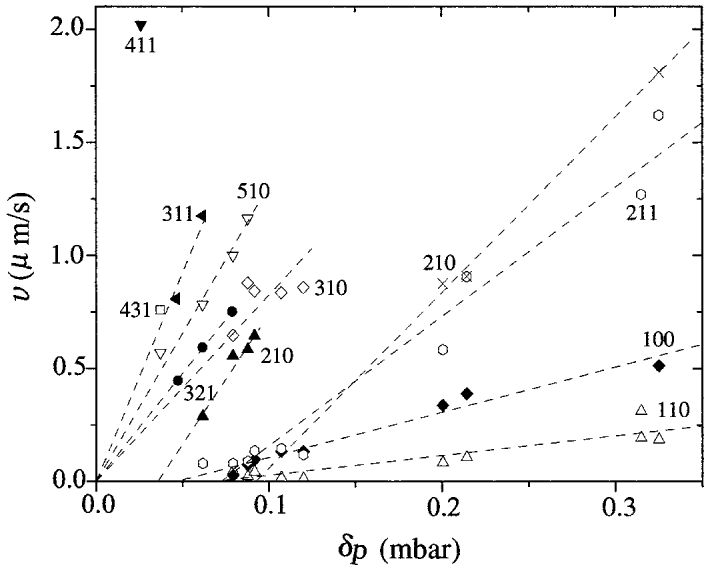

Fig. 14. Growth anisotropy of a single ^{3}He crystal measured at 0.55 mK. The dashed lines are the linear fits to the data for different facets marked with Miller indices.[44]

practically a linear dependence. Obvious is also a strong growth anisotropy, the velocities of the (510) and (110) facets, for instance, differ by an order of magnitude. These results can be explained by spiral growth of the facets in the regime of the so-called suppressed step mobility.[44] Assuming this growth mechanism, the step free energies β of different facets were calculated and the obtained energy values are plotted in Fig. 15 versus the corresponding step height d in log-log coordinates. A linear fit is consistent with the data and gives a fourth order power dependence ($\beta \propto d^4$). Such a dependence is expected for facets with sufficiently high Miller indices in the case when the elastic interaction between steps dominates at long distances, and the coupling between the liquid/solid interface and the crystal lattice is strong.[38] The large energies of steps on facets with low Miller indices, (110) and (100), also indicate strong coupling. This finding is surprising because it has been assumed that due to the higher amplitude of zero-point motion of ^{3}He atoms in the crystal lattice compared with ^{4}He, this coupling is very weak in ^{3}He.

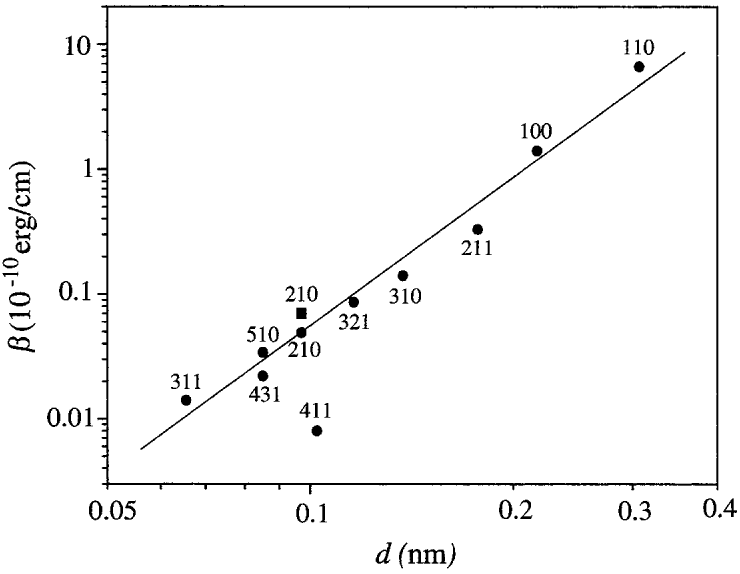

Fig. 15. Step free energies β of different facets calculated from the data in Fig. 14. The linear fit has a slope very close to four.[44]

3.2.3. Present studies with ^{3}He crystals

The facets disappear from the crystal surface at the so-called roughening transitions.[32] Every type of facets has its own roughening transition temperature and above all roughening transitions the equilibrium crystal shape is rounded and looks like a honey droplet at a table.[45] On ^{3}He crystals, no facets have been detected above 100 mK. It is believed, however, that the roughening transition of the (110) facets (which have the largest interplanar distance in the bcc-lattice) is at a much higher temperature of 260 mK as deduced from the surface tension measurements by Rolley *et al.*[45]

In order to clear the situation a systematic study of the shape and growth dynamics of ^{3}He crystals near 100 mK has been recently carried out in LTL. In this temperature range, additionally to the large latent heat of crystallization, the thermal conductivity of the normal ^{3}He liquid is very poor and the dynamics of crystals is slow as in ordinary crystals. Preliminary studies about this subject have been published in a short report.[46]

With ^{3}He crystals, magnetic properties can also be studied thanks to a nonzero nuclear spin of ^{3}He atom. The nuclear spin system of solid ^{3}He orders antiferromagnetically below the Néel temperature ($T_N = 0.93$ mK at the melting curve) and the spins form an up-up-down-down structure.[47] It

would be natural to expect a polarization induced change in facet mobilities at the magnetic ordering transition. The growth dynamics of the two basic types of facets on bcc ^{3}He crystals, (110) and (100), has been investigated near T_N, and it has been found that the magnetic ordering transition indeed has an effect on the mobility of the (100) facets.[48]

3.2.4. Future Plans

The equilibrium shape of ^{3}He crystals has been measured only near the melting curve minimum of 320 mK, where the latent heat of crystallization is small. The crystals looked rounded and it has been possible to extract the surface tension value of ^{3}He crystals by fitting the crystal surface profile with the Laplace-Young equation.[45] In ^{3}He another temperature region with small latent heat of crystallization exists well below T_N (i.e., in the ordered state of solid ^{3}He), where additionally the good thermal conductivity of superfluid ^{3}He would be helpful to measure the equilibrium shape of a faceted ^{3}He crystal which has never been done. According to the measurements on the step free energy on ^{3}He crystals at 0.55 mK performed in LTL, the basic facets should be quite large at these ultra low temperatures. The equilibrium size of the (110) facets, for instance, is expected be about 1/3 of the characteristic size of the crystal. Thus one of the next tasks is to measure the equilibrium shape of ^{3}He crystals at the lowest possible temperature. One has to note here that this kind of measurements require a good isolation of the experimental cell from the fluctuations taking place in the fill lines.

Also the feasibility of a possible observation of crystallization waves in ^{3}He could be estimated if temperatures well below 0.5 mK could be reached. These spectacular waves propagate on the superfluid/solid interface of ^{4}He and these waves should exist also in ^{3}He below 0.2 mK. It has been predicted also that in a magnetic field the propagating crystallization wave produces in ^{3}He bulk spin supercurrents, which result in a significant change of the wave spectrum.[49]

In a further perspective, it would be very interesting to study the growth dynamics of ^{3}He crystals in a magnetic field. At fields above 0.4 T the high-field spin-ordered phase of solid ^{3}He should be investigated as very little is known about that phase. For these measurements with a magnetic field, a new experimental cell has to be designed and built. Meanwhile, a systematic search for new facets on ^{4}He crystals could be carried out with the present setup as the Fabry-Pérot type of multiple-beam interferometer is very suitable for such kind of studies. With ^{4}He crystals, due to their fast dynamics, a faster CCD-camera is needed for imaging.

4. CONCLUSIONS

To conclude, one has to say that the interferometric techniques, applied and developed in LTL at ultra low temperatures, have proved to be a powerful tool to study various helium interfaces. Most of experimental findings have been really unique and have determined the world level of studies in the corresponding field. The present ongoing studies with ^{3}He crystals are not an exception in that respect and new exciting phenomena might be waiting just around the corner to be discovered.

ACKNOWLEDGMENTS

We would like to thank A.J. Manninen, J.P. Pekola, and I.A. Todoshchenko for useful discussions. This work was supported by the ULTI III (HPRI-1999-CT-0000) grants of the European Union) and the Academy of Finland [Finnish Centre of Excellence Programme (2000-2005)] and by INTAS grant 96-610.

REFERENCES

1. P.J. Hakonen, O.T. Ikkala, S.T. Islander, O.V. Lounasmaa, T.K. Markkula, P.M. Roubeau, K.M. Saloheimo, G.E. Volovik, E.L. Andronikashvili, D.I. Garibashvili, and J.S. Tsakadze, *Phys. Rev. Lett.* **48**, 1838 (1982).
2. For a semipopular review, see O.V Lounasmaa and E. Thuneberg, *Proc. Natl. Acad. Sci. USA* **96**, 7760 (1999).
3. See, e.g., E. Rolley, C. Guthmann, E. Chevalier, and S. Balibar, *J. Low Temp. Phys.* **99**, 851 (1995).
4. R. Wagner, P.J. Ras, P. Remeijer, S.C. Steel, and G. Frossati, *J. Low Temp. Phys.* **95**, 715 (1994).
5. R. van Rooijen, A. Marchenkov, H. Akimoto, O. Andreeva, P. van de Haar, R. Jochemsen, and G. Frossati, *J. Low Temp. Phys.* **124**, 497 (2001).
6. A.J. Manninen, H. Alles, A.V. Babkin, and J.P. Pekola, *Physica B* **178**, 352 (1992).
7. A.J. Manninen, J.P. Pekola, G.M. Kira, J.P. Ruutu, A.V. Babkin, H. Alles, and O.V. Lounasmaa, *Phys. Rev. Lett.* **69**, 2392 (1992).
8. D.V. Osborne, *Proc. Phys. Soc. London Sect. A* **63**, 909 (1950).
9. J.P. Ruutu, H. Alles, A.V. Babkin, P.J. Hakonen, and E. Sonin, *Europhys. Lett.* **28**, 163 (1994).
10. H. Alles, J.P. Ruutu, A.V. Babkin, P.J. Hakonen, A.J. Manninen, and J.P. Pekola, *Rev. Sci. Instrum.* **65**, 1784 (1994).
11. H. Alles, J.P. Ruutu, A.V. Babkin, P.J. Hakonen, O.V. Lounasmaa, and E.B. Sonin, *Phys. Rev. Lett.* **74**, 2744 (1995).
12. K.C. Harvey and A.L. Fetter, *J. Low Temp. Phys.* **11**, 473 (1973).

13. E.B. Sonin and A.J. Manninen, *Phys. Rev. Lett.* **70**, 2585 (1993).
14. H. Alles, J.P. Ruutu, A.V. Babkin, and P.J. Hakonen, *Phys. Rev. Lett.* **73**, 1388 (1994).
15. H. Alles, A.V. Babkin, P.J. Hakonen, J.P. Ruutu, J.T. Salojärvi, and J.P. Saramäki, *J. Low Temp. Phys.* **102**, 21 (1996).
16. R. Luusalo, A. Husmann, J. Kopu, and P.J. Hakonen, *Europhys. Lett.* **50**, 222 (2000).
17. J.P. Ruutu, P.J. Hakonen, A.V. Babkin, A.Ya. Parshin, and G. Tvalashvili, *J. Low Temp. Phys.* **112**, 117 (1998).
18. Manufactured by Photometrics, Tucson, Arizona, USA.
19. G.C. Straty and E.D. Adams, *Rev. Sci. Instrum.* **40**, 1393 (1969).
20. Manufactured by Andeen-Hagerling, Inc., Celveland, Ohio, USA.
21. V.I. Marchenko and A.Ya. Parshin, *Zh. Eksp. Teor. Fiz.* **79**, 257 (1980) [*Sov. Phys. JETP* **52**, 129 (1980)]; C. Jayaprakash, W.F. Saam, and S. Teitel, *Phys. Rev. Lett.* **50**, 2017 (1983).
22. A.V. Babkin, H. Alles, P.J. Hakonen, A.Ya. Parshin, J.P. Ruutu, and J.P. Saramäki, *Phys. Rev. Lett.* **75**, 3324 (1995).
23. M. Uwaha and P. Nozières, *J. Phys. Paris* **48**, 407 (1987); E.V. Thuneberg, *J. Low Temp. Phys.* **106**, 575 (1997).
24. A.F. Andreev, *Zh. Eksp. Teor. Fiz.* **106**, 1219 (1994) [*Sov. Phys. JETP* **79**, 660 (1994)].
25. O.L. Alerhand, D. Vanderbilt, R.D. Meade, and J.D. Joannopulos, *Phys. Rev. Lett.* **61**, 1973 (1998).
26. A.F. Andreev, *Pis'ma Zh. Eksp. Teor. Fiz.* **52**, 1204 (1990) [*JETP Lett.* **52**, 619 (1990)].
27. A.Ya. Parshin, *Physica B* **210**, 383 (1995).
28. H. Alles, A.V. Babkin, P.J. Hakonen, J.P. Ruutu, J.P. Saramäki, and A.Ya. Parshin, *J. Low Temp. Phys.* **101**, 519 (1995).
29. I.M. Lifshitz and Yu. Kagan, *Zh. Eksp. Teor. Fiz.* **62**, 385 (1972) [*Sov. Phys. JETP* **35**, 206 (1972)].
30. S. Balibar, T. Mizusaki, and Y. Sasaki, *J. Low Temp. Phys.* **120**, 293 (2000).
31. J.P. Ruutu, P.J. Hakonen, J.S. Penttilä, A.V. Babkin, J.P. Saramäki, and E.B. Sonin, *Phys. Rev. Lett.* **77**, 2514 (1996).
32. W.K. Burton, N. Cabrera and F.C. Frank, *Philos. Trans. R. Soc. London* **243A**, 299 (1951).
33. J.P. Ruutu, P.J. Hakonen, A.V. Babkin, A.Ya. Parshin, J.S. Penttilä, J.P. Saramäki, and G. Tvalashvili, *Phys. Rev. Lett.* **76**, 4187 (1996).
34. V. Tsepelin, J.P. Saramäki, A. Babkin, P.J. Hakonen, J.J. Hyvönen, R.M. Lusalo, A.Ya. Parshin, and G. Tvalashvili, *Phys. Rev. Lett.* **83**, 4804 (1999).
35. A.F. Andreev and L.A. Melnikovsky, *Zh. Eksp. Teor. Fiz.* **120**, 1457 (2001) [*Sov. Phys. JETP.* **93**, 1261 (2001)].
36. P.J. Hakonen, H. Alles, A. Babkin, and J.P. Ruutu, *J. Low Temp. Phys.* **101**, 41 (1995).
37. J.P. Härme, H. Alles, A. Babkin, R. Jochemsen, A.Ya. Parshin, V. Tsepelin, and G. Tvalashvili, *Physica B* **284-288**, 349 (2000).
38. V. Tsepelin, H. Alles, A. Babkin, R. Jochemsen, A.Ya. Parshin, and I.A. Todoshchenko, *J. Low Temp. Phys.* **129**, 489 (2002).

39. I.A. Todoshchenko, H. Alles, A. Babkin, A.Ya. Parshin, and V. Tsepelin, *J. Low Temp. Phys.* **126**, 1449 (2002).
40. L.D. Landau, *Collected Papers* (Pergamon Press, Oxford, 1971).
41. P. Nozières, in *Solids Far from Equilibrium*, edited by C. Godrèche, Cambridge Univ. Press, Cambridge (1991).
42. V. Tsepelin, H. Alles, A. Babkin, J.P. Härme, R. Jochemsen, A.Ya. Parshin, and G. Tvalashvili, *Phys. Rev. Lett.* **86**, 1042 (2001).
43. H. Alles, V. Tsepelin, A. Babkin, R. Jochemsen, A.Ya. Parshin, and I.A. Todoshchenko, *J. Low Temp. Phys.* **124**, 189 (2001).
44. V. Tsepelin, H. Alles, A. Babkin, R. Jochemsen, A.Ya. Parshin, and I.A. Todoshchenko, *Phys. Rev. Lett.* **88**, 045302 (2002).
45. E. Rolley, S. Balibar, F. Gallet, F. Graner, and C. Guthmann, *Europhys. Lett.* **8**, 523 (1989).
46. I.A. Todoshchenko, H. Alles, H.J. Junes, A.Ya. Parshin, and V. Tsepelin, *Physica B* **329-333**, 3869 (2003).
47. D.D. Osheroff, M.C. Cross, and D.S. Fisher, *Phys. Rev. Lett.* **44**, 792 (1980).
48. I.A. Todoshchenko, H. Alles, H.J. Junes, A.Ya. Parshin, and V. Tsepelin, to be published.
49. A.F. Andreev, *Physica B* **210**, 378 (1995).